

# SR-Stereo & DAPE: Stepwise Regression and Pre-trained Edges for Practical Stereo Matching

Weiqing Xiao, Wei Zhao\*

**Abstract**—Due to the difficulty in obtaining real samples and ground truth, the generalization performance and domain adaptation performance are critical for the feasibility of stereo matching methods in practical applications. However, there are significant distributional discrepancies among different domains, which pose challenges for generalization and domain adaptation of the model. Inspired by the iteration-based methods, we propose a novel stepwise regression architecture. This architecture regresses the disparity error through multiple range-controlled clips, which effectively overcomes domain discrepancies. We implement this architecture based on the iterative-based methods, and refer to this new stereo method as SR-Stereo. Specifically, a new stepwise regression unit is proposed to replace the original update unit in order to control the range of output. Meanwhile, a regression objective segment is proposed to set the supervision individually for each stepwise regression unit. In addition, to enhance the edge awareness of models adapting new domains with sparse ground truth, we propose Domain Adaptation based on Pre-trained Edges (DAPE). In DAPE, a pre-trained stereo model and an edge estimator are used to estimate the edge maps of the target domain images, which along with the sparse ground truth disparity are used to fine-tune the stereo model. The proposed SR-Stereo and DAPE are extensively evaluated on SceneFlow, KITTI, Middlebury 2014 and ETH3D. Compared with the SOTA methods and generalized methods, the proposed SR-Stereo achieves competitive in-domain and cross-domain performances. Meanwhile, the proposed DAPE significantly improves the performance of the fine-tuned model, especially in the texture-less and detailed regions. The code is available at <https://github.com/zhuxing0/SR-StereoV1-DAPE>.

**Index Terms**—Stereo matching, generalization performance, stepwise regression, domain adaptation.

## I. INTRODUCTION

**D**EPH information is key to computer vision and graphics research in the real world. Accurate depth estimation is vital for fields such as autonomous driving, robot navigation and action recognition. Common depth estimation methods include structured light [1], stereo matching [2], [4]–[7], and radar [3], etc. The structured light method projects a coded pattern onto the object surface and estimates the depth by observing the distortion of the pattern imaged on the object surface. Due to the need to project multiple patterns consecutively, structured light methods are generally only suitable for static indoor scenes. The radar obtains a sparse depth map by transmitting pulses and receiving echoes. Millimeter-wave radar has a long detection range but fuzzy spatial resolution,

*Corresponding author: Wei Zhao.*

Weiqing Xiao and Wei Zhao are with the School of Electronic and Information Engineering, Beihang University, Beijing 100191, China (e-mail: xiaowqtx@buaa.edu.cn; zhaowe1203@buaa.edu.cn)

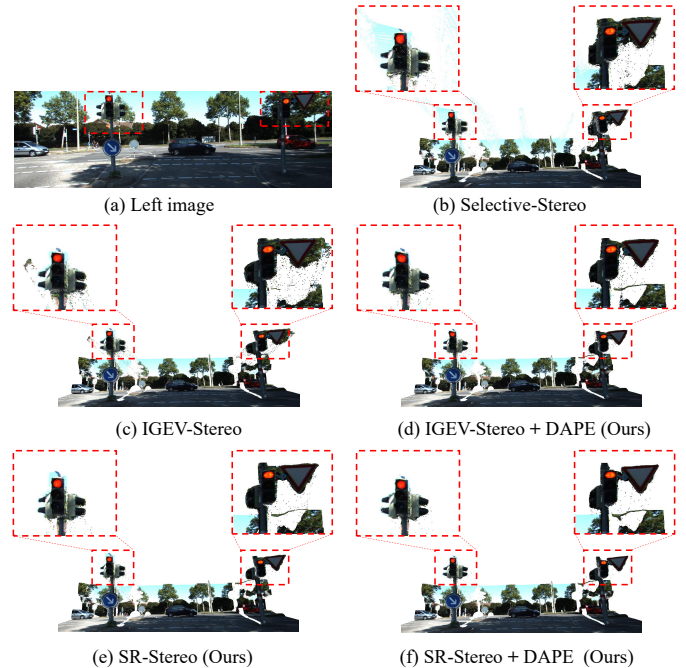


Fig. 1. Comparison of reconstructed point clouds on KITTI. All methods are trained on SceneFlow and fine-tuned on KITTI. During inference, all methods run 15 disparity updates. Our SR-Stereo performs better in the detailed regions. In addition, the proposed fine-tuning framework DAPE effectively improves the performance of existing methods fine-tuned on sparse ground truth.

while laser radar has a high spatial resolution but is expensive. In contrast, stereo matching calculates the depth map by estimating the horizontal displacement map (i.e., the disparity) of the pixels between the corrected left and right image pairs. By utilizing only two cameras, stereo matching is able to provide dense depth maps in different scenes, and is therefore considered a cost-effective and widely applicable method for depth estimation.

Many learning-based stereo methods [4]–[13] have achieved encouraging success. Some works [5]–[7] focus on designing the 4D cost volume, which characterizes the cost of pixel matching between left and right image pairs. They use 3D convolutional networks to aggregate and regularize the entire cost volume, and regress it to obtain the disparity. Recently, iteration-based methods [8]–[13] have shown great potential in terms of both accuracy and real-time performance, and thus have become the mainstay of current research. The iteration-based methods use similarity features from the cost volume

to predict the disparity error for optimization of the disparity. This approach avoids the expensive cost of aggregating and regularizing cost volume and achieves a balance between performance and efficiency by controlling the number of iterations.

However, real training samples and ground truth is usually difficult to obtain for stereo methods in practical applications. Existing methods [14], [23]–[25] are generally pre-trained on a large synthetic dataset (e.g., SceneFlow [16]) and then fine-tuned or directly inferred on real datasets, which makes higher demands on the generalization performance and domain adaptation performance. In addition, there are significant distributional discrepancies among different datasets due to differences in scene and resolution. For example, the maximum disparity in the Middlebury [17] exceeds 250 pixels, while all the disparities in the KITTI [18], [19] are within 100 pixels. These discrepancies make it difficult for a method that performs well on one dataset to directly achieve the same performance on other datasets. Therefore, a new architecture needs to be designed to overcome the domain discrepancies to achieve better robustness.

Our architecture is inspired by iteration-based methods. Iteration-based methods aim to correct disparity by directly predicting the current disparity error using update units. However, influenced by the disparity distribution, the disparity errors tend to vary across domains, which limits the generalization performance of iteration-based methods. Additionally, tens of updates are usually required to obtain accurate results. Based on these observations, we propose a novel stepwise regression architecture. In this architecture, we split the disparity error into multiple segments with fixed ranges and use multiple update units to predict them separately. This architecture has the following advantages: 1) the segments are range-controlled and domain-independent, and thus easy to generalize. 2) it still requires only tens of updates, and does not introduce additional computational and time costs.

We implement this architecture on the basis of iteration-based methods, and refer to this new stereo method as SR-Stereo. Specifically, we propose a stepwise regression unit to replace the original update unit. The output of the stepwise regression unit is range-controlled rather than unconstrained as in the original update unit. Then, we propose a regression objective segment, which sets a separate regression objective for each stepwise regression unit based on the splitting result of the disparity error. Further, we introduce a Disparity Clip-Balanced Weight to improve the accuracy of the predicted segments in the stepwise regression units.

Furthermore, we observe that models fine-tuned with sparse ground truth suffer from severe edge blurring, i.e., edge disparity errors. As shown in Figure 1, even the state-of-the-art models [10], [11] in the KITTI online leaderboard fail to accurately estimate the edge disparity. This further limits the effectiveness of stereo methods in real-world applications, as the vast majority of efficient labeling methods (e.g., radar) can only obtain sparse ground truth. The most direct way to mitigate this problem is to introduce edge-dependent supervision, but current edge feature extraction methods [20]–[22] have difficulty in obtaining accurate and concise edge

information due to the overly sparse disparity ground truth and the interference of object textures in RGB images.

In this paper, we propose a novel model fine-tuning framework to address the problem of blurring in edge details, which we name Domain Adaptation based on Pre-trained Edge (DAPE). The two key observations behind this framework are: 1) in contrast to RGB images, in disparity, the texture of the object is weakened while concise edge information is highlighted. 2) for the model pre-trained with dense ground truth, its predicted disparity on new domains tends to have accurate edge contours. Therefore, we first propose a lightweight edge estimator that takes both disparity and RGB image as inputs to generate a dense edge map. This estimator, along with SR-Stereo, is pre-trained on a virtual dataset. We utilize the pre-trained SR-Stereo to generate the disparity map for the target domain, which is further fed into the edge estimator to predict the edge map. Then, the background pixels in the edge map are retained, while the foreground pixels are filtered out. Following UCFNet [14], these pixels are defined as pseudo-labels. Finally, we use the edge pseudo-labels as additional supervision during the model fine-tuning process, which effectively improves the model’s disparity estimation performance on edge details.

In summary, our main contributions are:

- We propose a novel stereo method called SR-Stereo. It splits the disparity error into multiple segments for regression, which effectively overcomes the domain discrepancies (i.e., differences in disparity distribution). More importantly, we propose a stepwise regression architecture, which provides a new implementation idea for generalized stereo matching.
- We propose a novel fine-tuning framework for real datasets, named DAPE. By employing generated edge pseudo-label to supervise the model fine-tuning process, the proposed DAPE effectively improves the disparity estimation performance of models fine-tuned with sparse ground truth.
- We perform extensive experiments on SceneFlow, KITTI, Middlebury and ETH3D. Compared to the state-of-the-art methods, our SR-Stereo achieves competitive performance on several benchmarks. Meanwhile, compared to the majority of generalized stereo methods, our SR-Stereo achieves the best performance on Middlebury and ETH3D. The generalization performance of our method on KITTI is also very competitive among the methods of the last two years. In addition, experimental results on multiple realistic datasets show that DAPE significantly improves the performance of the fine-tuned model, especially in texture-less and detailed regions.

## II. RELATED WORK

### A. Iterative-based Stereo Matching

Compared to cost aggregation-based methods, iteration-based methods [23], [24] achieve significant improvement in both efficiency and accuracy. RAFT-Stereo [9] is the first iteration-based method that innovatively introduces multi-level GRU [27] (Gated Recurrent Unit) to update disparities in

stereo matching. Based on RAFT-Stereo, DLNR [13] replaces GRU with decoupled LSTM [28] (Long Short-Term Memory) to retain more high-frequency information during the iterative process, and designs a normalized refinement module to capture more detailed information at full resolution. Furthermore, CREStereo [8] applies the iterative process to different resolutions of disparity and proposes a hierarchical refinement network to update disparities in a coarse-to-fine manner. IGEV-Stereo [10] constructs a combined geometric encoding volume by combining Geometric Encoding Volume and All-Pairs Correlation, and uses a lightweight 3D regularization network to regress a rough initial disparity, which effectively improves the iterative efficiency and accuracy. Selective-Stereo [11] further enhances performance by extracting disparity information of different frequencies using GRUs with varying kernel sizes. Overall, these methods aim to directly regress the entire disparity error to achieve fast disparity optimization. In contrast, our SR-Stereo does not insist on directly regressing the disparity error, but instead splits it into multiple range-controlled and domain-independent segments to overcome the distributional discrepancies among different domains.

### B. Generalized Stereo Matching and Domain Adaptation

Several works have focused on cross-domain generalization and domain adaptation. UCFNet [14] narrows domain discrepancies by refining disparities in stages and adaptively adjusts the disparity search space at each stage through uncertainty estimation. Additionally, it proposes a fine-tuning framework based on pseudo-labels of target domain disparities to enhance the model’s domain adaptation performance. HVT [39] enriches the distribution of training data by transforming a synthetic dataset at three levels (global, local, and pixel), thereby improving the model’s generalization ability. Graft-Net [37] incorporates broad-spectrum features from a large-scale dataset into stereo matching to enhance the model’s robustness to image styles. Rao et al. [40] enhance the learning of structural information by integrating stereo matching and image reconstruction tasks, thereby improving the model’s generalization performance. Zhang et al. [38] explicitly constrain the feature consistency of matching pixel pairs by introducing a stereo contrastive feature loss function. DKT [36] introduces a teacher-student architecture, which analyzes the differences between ground truth labels and pseudo-labels to enhance the model’s robustness. In contrast, our SR-Stereo focuses on constructing domain-independent regression objectives, specifically by predicting range-controlled disparity error segments to achieve more robust performance.

In addition, making good use of the few real samples is important for domain adaptation of the model. Some works [9]–[11] have demonstrated that even using only a few samples, the performance of pre-trained models in a new domain can be significantly improved. However, these methods simply fine-tune the model using the ground truth disparity of the new domain, without considering the impact of ground truth density on domain adaptation. For instance, models fine-tuned with sparse ground truth often suffer from severe edge blurring. EdgeStereo [41] mitigates this issue by integrating stereo

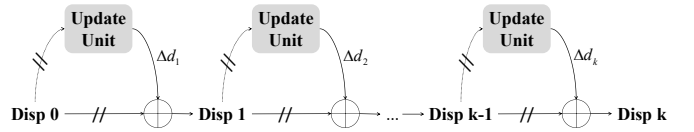


Fig. 2. The disparity update process of iteration-based methods. In this process, the update unit outputs the residual disparity to update the current disparity. The // means stop gradient.

matching and edge detection tasks. Our DAPE provides a simpler solution by using a pre-trained stereo model and edge estimator to offer additional edge supervision for model fine-tuning. In contrast to EdgeStereo, the stereo model and edge estimator in DAPE are completely decoupled, thus avoiding unnecessary overhead during the inference.

## III. METHODOLOGY

### A. Overview

In this chapter, we provide a novel and complete solution for cross-domain generalization and domain adaptation for stereo methods. Firstly, we propose a novel stereo method, SR-Stereo, which overcomes the domain discrepancies by regressing multiple range-controlled disparities. Then, we propose a general and reliable framework, DAPE, for domain adaptation on sparse ground truth.

Objectively, SR-Stereo and DAPE are independent, i.e., they can be used independently to solve specific problems. In Section III-B, we describe the principle of existing iteration-based methods and highlight the essential improvements introduced by the proposed SR-Stereo. In Section III-C and Section III-D, we describe the proposed SR-Stereo and DAPE in detail.

### B. Preliminaries

Distinct from the cost aggregation-based methods, the iteration-based methods employ update units to predict and optimize the disparity. Ignoring steps such as upsampling, the disparity update can be roughly summarized by the process in Figure 2. Obviously, the whole process can be formulated as:

$$d_k = d_{k-1}^* + \Delta d_k \quad (1)$$

where  $d_k$  denotes the predicted disparity after  $k$  iterations,  $\Delta d_k$  denotes the residual disparity in the  $k$ -th iteration, and  $*$  denotes no gradient. Then, during training, all the predicted disparities are supervised:

$$Loss = \sum_{k=1}^N \gamma_k \|d_{gt} - d_k\| \quad (2)$$

where  $Loss$  denotes the training loss,  $d_{gt}$  denotes the ground truth disparity,  $\gamma_k$  is the loss weight (hyperparameter) and  $\|\cdot\|$  denotes common loss functions (e.g., L1, SmoothL1, etc.). Considering Eq 1, the supervision in Eq 2 can be equated:

$$Loss = \sum_{k=1}^N \gamma_k \|d_{k-1}^{error} - \Delta d_k\| \quad (3)$$

in which

$$d_{k-1}^{error} = d_{gt} - d_{k-1}^* \quad (4)$$

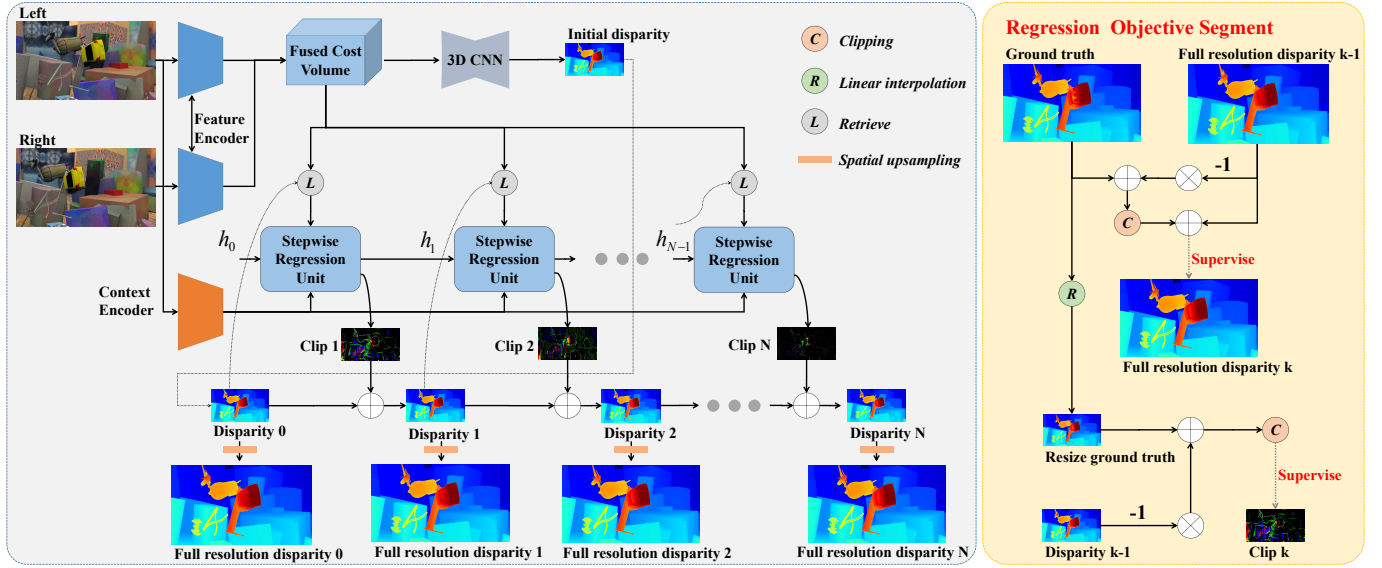


Fig. 3. The overall architecture of the proposed SR-Stereo. Compared to iteration-based methods, SR-Stereo is specially designed in terms of the update unit and the regression objective. Specifically, we propose a stepwise regression unit that outputs range-controlled disparity clips, rather than unconstrained residual disparities. Further, we design separate regression objectives for each stepwise regression unit, instead of simply using the disparity error.

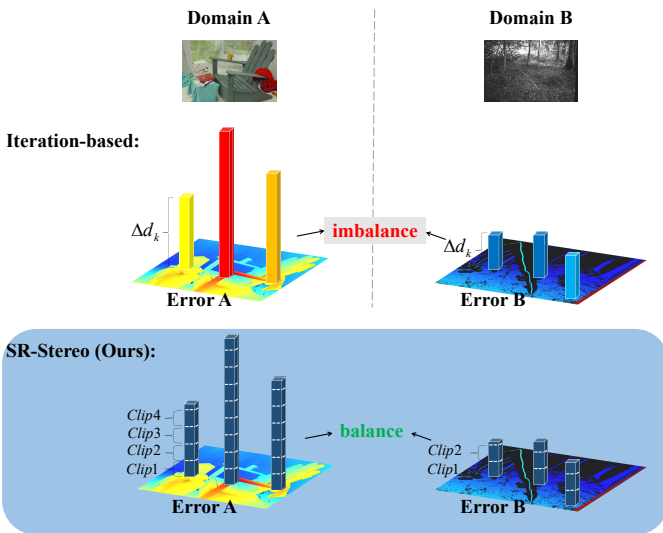


Fig. 4. Visualization of the regression objectives of SR-Stereo and iteration-based methods. The iteration-based methods regress disparity error by predicting residual disparity  $\Delta d_k$ , while SR-Stereo splits the disparity error into multiple segments and regresses them by predicting multiple disparity clips.

Essentially, the core of the iteration-based methods is the regression of the residual disparity  $\Delta d_k$  to the disparity error  $d_{gt} - d_{k-1}^*$ . In contrast, in our SR-Stereo, the disparity error is split into multiple range-controlled segments for regression, thus mitigating the domain discrepancies, as shown in Figure 4. In this paper, we reconstruct the update unit and regression objective in existing iteration-based methods to implement SR-Stereo. To highlight the differences, we refer to the output of the new update unit as a disparity clip rather than residual disparity.

### C. Stepwise Regression Stereo

In this section, we describe the key components that implement SR-Stereo and show how they can be plugged into iteration-based methods. Using IGEV-Stereo [10] as the basic model, the overall architecture is shown in Figure 3. Intuitively, we retain the original feature extraction and cost-volume construction, but reconstruct the update unit and its regression objective. In addition, we propose a loss weight for the new update unit that is related to the regression objective scale.

1) *Feature extraction and Cost volume Construction:* We do not change the feature extraction and cost-volume construction of IGEV-Stereo [10], but still describe them in this subsection.

*Feature Encoder.* We use MobileNetV2 [29] pre-trained on ImageNet [30] and a series of upsampling blocks to extract multi-scale features  $f_1^{left,i} \in \mathbb{R}^{C_i \times H/2^{i+1} \times W/2^{i+1}}$  from the left image  $I_{left} \in \mathbb{R}^{3 \times H \times W}$  and  $f_1^{right,i} \in \mathbb{R}^{C_i \times H/2^{i+1} \times W/2^{i+1}}$  from the right image  $I_{right} \in \mathbb{R}^{3 \times H \times W}$ , respectively. The  $i = 1, 2, 3, 4$  and the feature size  $C_i = 48, 64, 192, 160$ .

*Context Encoder.* We use a series of residual blocks [31] and downsampling layers to extract multi-scale context features  $f_2^{left,j} \in \mathbb{R}^{C_j \times H/2^{j+1} \times W/2^{j+1}}$  ( $j=1,2,3,4$  and  $C_j=128$ ) from the left image. These features are inserted into the stepwise regression unit to provide global information.

*Cost Volume.* By combining Geometry Encoding Volume (GEV) and All-pairs Correlations (APC), we construct the cost volume  $G_c$  based on  $f_1^{left,1}$  and  $f_1^{right,1}$ . Then, we use a lightweight 3D UNet to aggregate the GEV and obtain the initial disparity  $d_{init} \in \mathbb{R}^{1 \times H/4 \times W/4}$ .

2) *Stepwise Regression Architecture:* In this subsection, we detail the two key components that implement SR-Stereo: the stepwise regression unit and the regression objective segment.

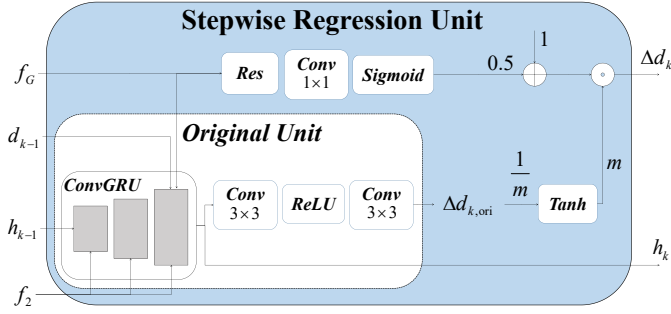


Fig. 5. Architecture of the stepwise regression unit. The  $m$  is the hyperparameter that controls the range of the output disparity clip. The  $\Delta d_{k,ori}$  is the residual disparity output of the original update unit, and  $Res$  is the residual layer.

*Stepwise Regression Unit.* Figure 5 shows the architecture of the stepwise regression unit, which highlights the improvements over the original update unit. For each regression, we index a set of features  $f_G$  from the cost volume  $G_c$  using the current disparity-centered set as follows:

$$f_G = \sum_{r=-4}^4 \text{concat} \{G_c(d_{k-1} + r), G_c^p(d_{k-1}/2 + r)\} \quad (5)$$

where  $d_{k-1}$  is the current disparity ( $d_0 = d_{init}$ ) and  $p$  denotes the average pooling operation. We use these features from  $G_c$  along with the current disparity  $d_{k-1}$  to update the hidden state  $h_{k-1}$  of ConvGRU [10]:

$$h_k = \text{ConvGRU}(f_G, d_{k-1}, h_{k-1}, f_2^{left}) \quad (6)$$

where  $h_k$  is the updated hidden state. Then, the  $h_k$  and  $f_G$  are passed into a series of convolutional layers and residual layers [31] to generate the disparity clip  $\Delta d_k \in \mathbb{R}^{1 \times H/4 \times W/4}$  as follows:

$$\Delta d_k = \tanh\left(\frac{\Delta d_{k,ori}}{m}\right) \times m \odot (1 + 0.5w) \quad (7)$$

in which

$$w = \sigma(\text{Conv}_{1 \times 1}(\text{Res}(f_G))) \quad (8)$$

$$\Delta d_{k,ori} = \text{Conv}_{3 \times 3}(\text{Relu}(\text{Conv}_{3 \times 3}(h_k))) \quad (9)$$

where  $\sigma$  denotes the sigmoid function,  $Res$  is the residual layer,  $\odot$  denotes the Hadamard product, and  $\Delta d_{k,ori} \in \mathbb{R}^{1 \times H/4 \times W/4}$  is the residual disparity output of the original update unit. We set the hyperparameter  $m$  to constrain the approximate range of the disparity clips, and use the weight map  $w$  to adaptively adjust the constraint magnitude for different regions. The weight map  $w$  is computed from the cost-volume feature.

Finally, we update the current disparity and use the Spatial Upsampling [10] to generate the full-resolution disparity  $d_k^{full} \in \mathbb{R}^{1 \times H \times W}$  as follows:

$$d_k = d_{k-1} + \Delta d_k \quad (10)$$

$$d_k^{full} = \text{Upsampling}(f_1^{left,i}, I_{left}, 4d_k) \quad (11)$$

*Regression Objective Segment.* We specify how to obtain the ground truth disparity clip  $\Delta d_{gt,k}$  and the full-resolution

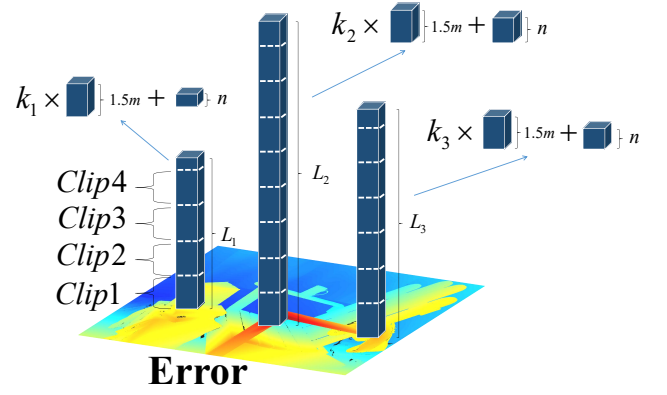


Fig. 6. Long-tailed distribution of regression objectives for disparity clips. SR-Stereo regresses the disparity error by predicting multiple disparity clips, but the regression objectives of disparity clips are long-tailed.

ground truth disparity  $d_{gt,k}^{full}$ . Specifically, the ground truth of the full-resolution disparity is constantly changing with the stepwise regression process, as shown below:

$$d_{gt,k}^{full} = d_{k-1}^{full} + \text{clip}_{-6m}^{6m}(d_{gt} - d_{k-1}^{full}) \quad (12)$$

in which

$$\text{clip}_{-M}^M(x) = \begin{cases} -M & \text{if } x < -M \\ x & \text{if } -M \leq x \leq M \\ M & \text{if } x > M \end{cases} \quad (13)$$

where  $d_{gt}$  is the ground truth disparity and  $\text{clip}$  denotes the clipping operation.

In addition, we use linear interpolation to generate the ground truth disparity clip  $\Delta d_{gt,k}$ :

$$\Delta d_{gt,k} = \text{clip}_{-1.5m}^{1.5m}\left(\frac{\text{Resize}(d_{gt})}{4} - d_{k-1}\right) \quad (14)$$

where  $\text{Resize}$  denotes linear interpolation downsampling. We point out that supervision of the disparity clips is not necessary, but slightly improves the model's performance (see Section IV-C for experimental results).

3) *Disparity Clip-Balanced Weight:* As mentioned earlier, SR-Stereo mitigates the domain discrepancies by predicting multiple disparity clips to regress the disparity error. However, this approach leads to a new problem: the regression objective for the disparity clips exhibits a long-tailed distribution, as shown in Figure 6. Ideally, a disparity error of size  $L$  can be regressed by multiple clips of size  $1.5m$  and a small clip of size  $n$  as follows:

$$L = k \times 1.5m + n \quad (15)$$

where  $k \in \mathbb{Z}$  and  $n \in (0, 1.5m)$ . Obviously, the distribution of regression objectives is long-tailed (especially when the disparity error is large), which limits the accuracy of small disparity clips. In this paper, a Disparity Clip-Balanced Weight is proposed to mitigate the long-tailed distribution. The formula for this weight is as follows:

$$w_{balanced}(x) = \text{clip}_0^{1.5}(|x|^{-h}) \quad (16)$$

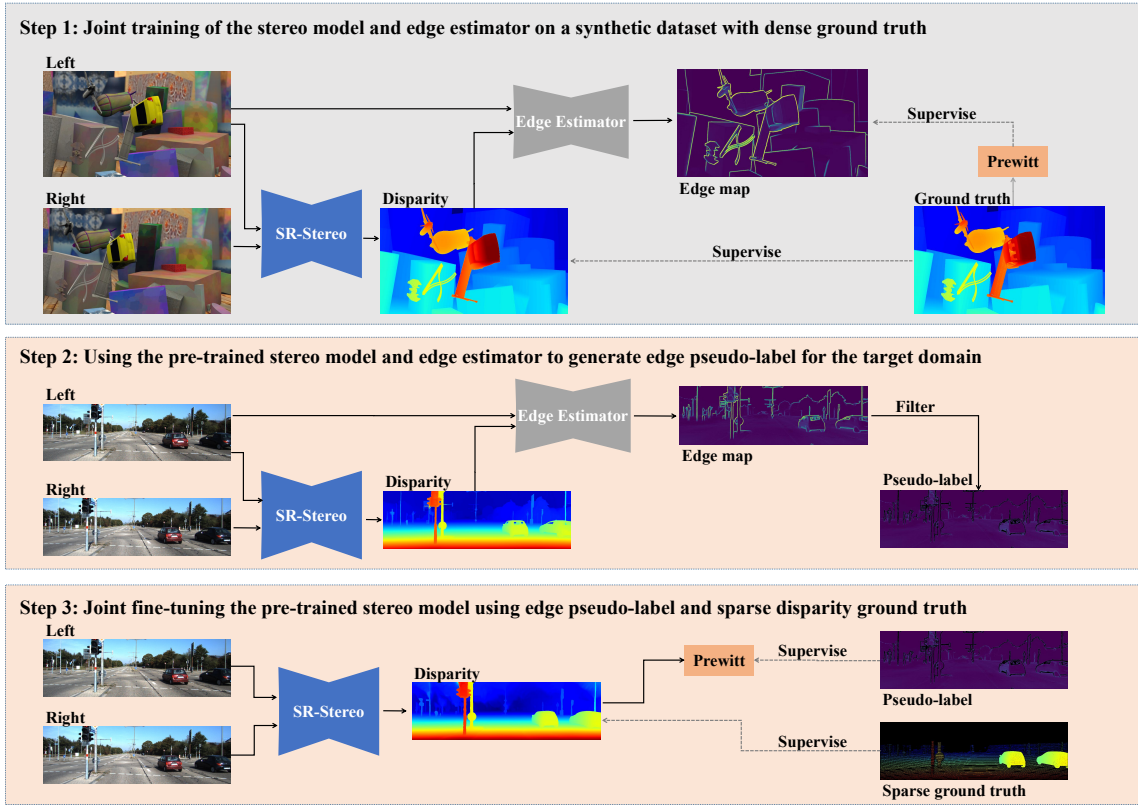


Fig. 7. The overall framework of the proposed DAPE. First, a robust stereo model SR-Stereo and a lightweight edge estimator are pre-trained on a large synthetic dataset with dense ground truth. Then, we use the pre-trained SR-Stereo and edge estimator to generate the edge map of target domain, where the background pixels (i.e., non-edge region pixels) are used as edge pseudo-labels. Finally, we jointly fine-tune the pre-trained SR-Stereo using the edge pseudo-labels and sparse ground truth disparity.

where  $h$  is a hyperparameter that controls the bias towards small disparity clip. This weight can be flexibly inserted into existing loss functions:

$$CB_{L1}(x) = w_{balanced}(x) \times |x| \quad (17)$$

$$CB_{SmoothL1}(x) = \begin{cases} w_{balanced}(x) \times 0.5x^2 & \text{if } x < 1 \\ w_{balanced}(x) \times |x| & \text{otherwise} \end{cases} \quad (18)$$

4) *Loss Function*: We use Smooth L1 loss to supervise the initial disparity and the disparity clips  $\Delta d_k$ :

$$Loss_{init} = Smooth_{L1}(d_{init}^{full} - d_{gt}) \quad (19)$$

$$Loss_{\Delta d} = \sum_{k=1}^N \gamma^{N-k} CB_{SmoothL1}(\Delta d_k - \Delta d_{gt,k}) \quad (20)$$

where  $\gamma = 0.9$  and  $N$  is the total number of disparity clips. We use L1 loss to supervise full-resolution disparities:

$$Loss_{full} = \sum_{k=1}^N \gamma^{N-k} CB_{L1}(d_k^{full} - d_{gt,k}^{full}) \quad (21)$$

Ultimately, the total loss function for SR-Stereo is as follows:

$$Loss_{total} = Loss_{init} + Loss_{\Delta d} + Loss_{full} \quad (22)$$

#### D. Domain Adaptation based on Pre-trained Edge

We propose a Domain Adaptation based on Pre-trained Edge (DAPE) to mitigate edge blurring for model fine-tuned with sparse ground truth. As shown in Figure 7, the proposed DAPE consists of three steps:

- 1) Firstly, a robust stereo model and a lightweight edge estimator are pre-trained on a large synthetic dataset (i.e., the source domain) with dense ground truth. Specifically, the input to the edge estimator is the disparity predicted by the stereo model along with the RGB image.
- 2) Then, the pre-trained stereo model and the edge estimator are used to directly infer on the target domain and generate corresponding edge maps. To mitigate the negative impact of disparity errors in reflective regions, we recommend using only the relatively dense background pixels (i.e., non-edge region pixels) from the edge maps as pseudo-labels (following UCFNet [14], these pixels are defined as pseudo-labels).
- 3) After generating the edge pseudo-labels of the target domain, we use it and the sparse ground truth disparity to jointly fine-tune the pre-trained stereo model.

In the following, we describe the edge estimator, the edge map background pseudo-labels and the joint fine-tuning process in detail.

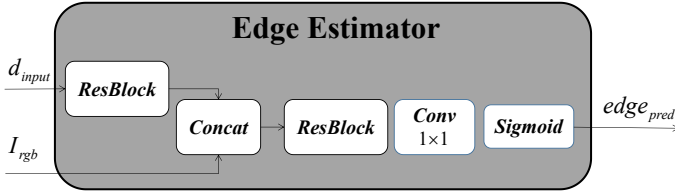


Fig. 8. Architecture of the edge estimator. The entire network consists of only two residual blocks and one convolution block.

1) *Edge Estimator*: For the proposed DAPE, the reliability of edge pseudo-label is vital to the performance of the fine-tuned model. Existing edge estimation methods usually take only an RGB image as input and use a series of complex 2D CNNs to estimate the contour of object by extracting high-level features. However, this approach significantly increases the computational cost and limits the generalization performance due to the substantial differences in object categories and distributions across different domains.

In this paper, we claim that using disparity for edge estimation is a better and more robust approach because disparity estimation focuses on local geometric information, whose representations are similar among different domains. Moreover, compared to RGB image, disparity contains almost no object texture information, which greatly reduces the difficulty of edge estimation. Thus, a lightweight edge estimator is proposed to achieve accurate and robust edge prediction by introducing disparity. The architecture of the edge estimator is shown in Figure 8. First, a residual block is used to extract the edge feature in the disparity:

$$f_{edge} = ResBlock(d_{input}) \quad (23)$$

where  $ResBlock$  denotes the residual block,  $d_{input}$  is the disparity, and the number of channels for  $f_{edge}$  is 29. In order to mitigate the potential effects of noise in the disparity, the RGB image is used to refine the edge feature map. Specifically, the edge feature and the corresponding RGB image are passed together to a residual block to achieve feature refinement. Finally, we use a  $1 \times 1$  convolutional layer and a sigmoid layer to generate the refined edge map as follows:

$$f_{refine} = ResBlock(concat(f_{edge}, I_{rgb})) \quad (24)$$

$$edge_{pred} = \sigma(Conv_{1 \times 1}(f_{refine})) \quad (25)$$

where  $edge_{pred}$  is the predicted edge map,  $I_{rgb}$  is the RGB image corresponding to the disparity,  $\sigma$  denotes the sigmoid function, and the number of channels of  $f_{refine}$  is 16.

*Loss Function*. We use Smooth  $L1$  loss to train the proposed edge estimator on a large synthetic dataset:

$$Loss_{edge} = Smooth_{L1}(edge_{pred} - edge_{gt}) \quad (26)$$

where  $edge_{gt}$  is the ground truth edge map. Since the ground truth edge map is not provided in the dataset, we use the Prewitt operator to extract the edge of the ground truth disparity as  $edge_{gt}$ :

$$edge_{gt} = \begin{cases} 1 & \text{if } Prewitt(d_{gt}) > 5 \\ 0 & \text{otherwise} \end{cases} \quad (27)$$

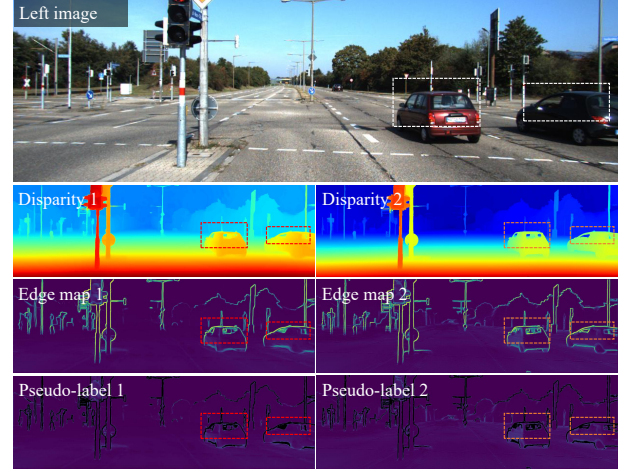


Fig. 9. Generalization results of existing methods on KITTI 15. The labels 1 and 2 in the figure denote the IGEV-Stereo and the proposed SR-Stereo, respectively. The edge map is represented using a pseudo-color image, where the black color indicates the invalid regions. As shown, the existing methods perform poorly in reflective regions, which leads to wrong edges. Therefore, we propose to use only pixels in non-edge region as pseudo-label.

where  $d_{gt}$  is the ground truth disparity and  $Prewitt$  denotes the Prewitt operator.

2) *Edge Map Background Pseudo-label Generation for Target Domain*: The proposed edge estimator achieves edge estimation by introducing disparity, and therefore is affected by the accuracy of the disparity. As shown in Figure 9, existing disparity estimation methods perform badly in reflection regions, which leads to erroneous edges. In this paper, an edge map background pseudo-label is proposed to generate reliable supervision for fine-tuning. Intuitively, in an ideal edge map, both the edge region and non-edge region can be leveraged as supervision to improve the performance of the fine-tuned disparity estimation model. For instance, the disparity map typically exhibits high gradients in edge region, while it remains relatively flat in non-edge region. Erroneous edges in reflection regions do not affect the reliability of the pixels in the non-edge region. Therefore, we can simply utilize pixels in non-edge region as the pseudo-label (i.e., the edge map background pseudo-label):

$$edge_{background} = \{p < t \mid p \in edge_{pred}\} \quad (28)$$

where  $t$  is the threshold that controls the density of non-edge region.

3) *Joint Fine-tuning on the Target Domain*: After obtaining the edge map background pseudo-label, we use it and the sparse ground truth disparity from the target domain as supervision to jointly fine-tune the pre-trained stereo matching model. Specifically, we propose an edge-aware loss to improve the detail of the predicted disparity as follows:

$$Loss_{edge} = Smooth_{L1}(edge_{d_{pred}} - edge_{background}) \quad (29)$$

where  $edge_{d_{pred}}$  is the edge map corresponding to predicted disparity  $d_{pred}$ . As in Section III-D1, we use the Prewitt operator to extract the edge map of the predicted disparity:

$$edge_{d_{pred}} = \sigma(10 \times (Prewitt(d_{pred}) - 5)) \quad (30)$$

The total loss of the joint fine-tuning process is shown below:

$$Loss_{DAPE} = Loss_{stereo} + Loss_{edge} \quad (31)$$

where  $Loss_{stereo}$  is the loss of the original stereo matching method, e.g., Eq 22.

#### IV. EXPERIMENTS

##### A. Datasets and Evaluation Metrics

**SceneFlow** [16] is a large synthetic dataset that consists of 35,454 training pairs and 4,370 testing pairs, with a resolution of  $960 \times 540$ . It provides dense ground truth for optical flow and stereo matching. We utilize this dataset to pretrain the proposed SR-Stereo and the edge estimator with 3-pixel error and end-point error (EPE) as evaluation metrics.

**Middlebury 2014** [17] consists of two batches of indoor image pairs. The first batch provides 15 training pairs and 15 test pairs, with each scene provided in three different resolutions. The second batch provides 13 additional training pairs, but contains only one resolution. All training pairs are provided with dense hand-labeled ground truth disparity, which ranges from 0 to 300. We directly use the training pairs from the first batch to evaluate the generalization performance of SR-Stereo. For DAPE, we utilize the additional 13 image pairs to fine-tune the model and evaluate its performance using the 15 training pairs from the first batch. The evaluation metric used is the 2-pixel error.

**ETH3D** [32] is a grayscale image dataset that includes a variety of indoor and outdoor scenes. It consists of 27 training pairs and 20 test pairs. The dataset provides sparsely labeled ground truth disparities for the training pairs, ranging from 0 to 60 (the smallest among several datasets). Similar to the usage in Middlebury 2014, we employ the training pairs to directly assess the generalization performance of the proposed method, using the 1-pixel error as the evaluation metric. Additionally, we use 14 training pairs as fine-tuning samples and 13 training pairs as test samples to evaluate the effectiveness of the proposed Domain Adaptation based on Pre-trained Edge.

**KITTI 2012** [19] and **KITTI 2015** [18] are datasets of real-world driving scenes. KITTI 2012 consists of 194 training pairs and 195 test pairs, while KITTI 2015 contains 200 training pairs and 200 test pairs. Both datasets provide sparse ground truth disparity (sparsest in several datasets) obtained using lidar. The disparity values range from 0 to 230. In Section IV-E2, we merge KITTI 2012 and KITTI 2015, referred to as **KITTI**. For evaluation, we adopt the 3-pixel error as the metric. To assess the efficacy of our proposed DAPE method, we allocate 80% of the KITTI training set for fine-tuning the model and reserve the remaining 20% for validation.

##### B. Implementation Details

In this paper, we implement the proposed methods using pytorch and conduct experiments using two NVIDIA RTX 3090 GPUs. For all the experiments, we use the AdamW optimizer and one-cycle learning rate schedule, as well as the same data augmentation strategies. Specifically, we preprocess the training pairs by applying the saturation transform and

randomly cropping them to ensure a consistent image size ( $320 \times 512$  for ETH3D,  $384 \times 1024$  for Middlebury 2014, and  $320 \times 672$  for other datasets). Below, we provide a detailed description of the training settings for SR-Stereo and DAPE, respectively.

1) **SR-Stereo**: In the experimental section, following Selective-Stereo [11] and MoCha-Stereo [33], we implement the proposed SR-Stereo on the basis of IGEV-Stereo for a fair comparison. All ablation versions of SR-Stereo are trained on SceneFlow with a batch size of 4 for 50k steps, while the final version of SR-Stereo (represented by SR-IGEV) is trained on SceneFlow with a batch size of 8 for 200k steps. The final model and ablation experiments are conducted using a one-cycle learning rate schedule with learning rates of 0.0002 and 0.0001, respectively. Following some generalized stereo methods [38]–[40], we directly evaluate cross-domain performance on the training sets of KITTI, Middlebury, and ETH3D.

2) **DAPE**: For the experiments related to the edge estimator, we jointly train the stereo model and edge estimator on SceneFlow with a batch size of 4 for 50k steps, using a one-cycle learning rate schedule with a learning rate of 0.0001. Then, we use the pre-trained stereo model and edge estimator to generate edge pseudo-labels for target domains. Following existing methods [8], [9], [13], we adopt different settings of fine-tuning process for different datasets. For the KITTI, we adopt a batch size of 4 and fine-tune the model for 50k steps with an initial learning rate of 0.0001. As for the ETH3D, we use a batch size of 2 and fine-tune the model for 2,000 steps, also with an initial learning rate of 0.0001. In the case of the Middlebury 2014, we utilize a batch size of 2 and fine-tune the model for 4,000 steps, starting with an initial learning rate of 0.00002.

##### C. Ablation Study

In this section, we explore the effectiveness and optimal configuration of each component of SR-Stereo.

1) **Stepwise Regression Architecture**: We explore the optimal settings for stepwise regression architecture as well as its effectiveness. Table I shows the results of stepwise regression architecture in different configurations. In the majority of configurations, the incorporation of stepwise regression architecture significantly enhances the performance of the baseline model across different datasets.

In lines (b) to (e), experiments conducted with varying ranges ( $m$ ) of disparity clips demonstrate that the choice of disparity clip range impacts the performance on different datasets. For datasets with a small range of disparity, smaller disparity clips are preferred, while datasets with a larger range of disparity benefit from larger disparity clips. Interestingly, the stepwise regression architecture achieves consistent and stable performance across all datasets when  $m = 2$ .

In lines (f) to (g), our method achieves further performance improvement through the supervision of disparity clips. By incorporating supervision specifically on disparity clips, the model’s accuracy and generalization capability are enhanced.

In lines (h) to (k), we investigate the impact of the number of stepwise regression units employed in the architecture.

TABLE I

ABLATION STUDY OF SR-STEREO. THE BASELINE (I.E. \*) IS IGEV-STEREO. THE  $num_{GRU}$  DENOTES THE USAGE TIMES OF CONVGRU, WHILE THE  $num_{SRU}$  DENOTES THE USAGE TIMES OF THE PROPOSED STEPWISE REGRESSION UNIT. ALL METHODS RUN 15 DISPARITY UPDATES DURING INFERENCE ( $num_{GRU} + num_{SRU} = 15$ ). THE FINAL CONFIGURATION OF  $m$  IS UNDERLINED. **BOLD**: BEST. **BLUE**: SECOND.

| Index | Variations  |             |          |                   | SceneFlow   |             | Middlebury-H | ETH3D       | Params.(M) |
|-------|-------------|-------------|----------|-------------------|-------------|-------------|--------------|-------------|------------|
|       | $num_{GRU}$ | $num_{SRU}$ | $m$      | $Loss_{\Delta d}$ | EPE(px)     | > 3px       | > 2px(%)     | > 1px(%)    |            |
| (a)*  | 15          | 0           | -        | -                 | 0.72        | 3.65        | 8.44         | 4.49        | 12.60      |
| (b)   | 0           | 15          | 1        | -                 | 0.71        | 3.61        | 8.42         | <b>4.10</b> | 12.77      |
| (c)   | 0           | 15          | 2        | -                 | <b>0.69</b> | <b>3.51</b> | 7.89         | 4.47        | 12.77      |
| (d)   | 0           | 15          | 3        | -                 | <b>0.70</b> | 3.55        | 7.66         | 4.44        | 12.77      |
| (e)   | 0           | 15          | 4        | -                 | <b>0.69</b> | 3.54        | <b>7.31</b>  | 5.14        | 12.77      |
| (f)   | 0           | 15          | <u>2</u> | ✓                 | <b>0.70</b> | <b>3.49</b> | <b>6.78</b>  | <b>4.05</b> | 12.77      |
| (g)   | 0           | 15          | 3        | ✓                 | <b>0.69</b> | <b>3.49</b> | 7.44         | 4.15        | 12.77      |
| (h)   | 4           | 11          | 2        | ✓                 | <b>0.69</b> | <b>3.49</b> | 7.50         | 4.61        | 12.77      |
| (i)   | 4           | 11          | 3        | ✓                 | <b>0.70</b> | 3.56        | 7.80         | 4.61        | 12.77      |
| (j)   | 8           | 7           | 2        | ✓                 | <b>0.69</b> | <b>3.49</b> | 7.77         | <b>4.10</b> | 12.77      |
| (k)   | 8           | 7           | 3        | ✓                 | <b>0.70</b> | 3.52        | 7.91         | 4.79        | 12.77      |

TABLE II

ABLATION STUDY OF DISPARITY CLIP-BALANCED WEIGHT. WE INTERPOLATE THE PROPOSED DISPARITY CLIP-BALANCED WEIGHT INTO THE LOSS FUNCTION OF SR-STEREO. ALL METHODS RUN 15 DISPARITY UPDATES DURING INFERENCE. THE FINAL CONFIGURATION OF THE  $h$  IS UNDERLINED. **BOLD**: BEST.

| Methods     | $h$        | SceneFlow   |             | Middlebury-F | ETH3D       |
|-------------|------------|-------------|-------------|--------------|-------------|
|             |            | EPE(px)     | > 3px       | > 2px        | > 1px       |
| IGEV-Stereo | -          | 0.72        | 3.65        | 17.47        | 4.49        |
| SR-Stereo   | -          | 0.70        | 3.49        | 14.99        | 4.05        |
|             | 0.1        | <b>0.69</b> | 3.44        | 14.74        | 3.93        |
|             | 0.3        | <b>0.69</b> | 3.32        | 14.90        | 4.18        |
|             | <u>0.5</u> | 0.70        | <b>3.23</b> | <b>14.23</b> | <b>3.82</b> |

Experimental results reveal that increasing the usage times of stepwise regression units leads to better generalization performance of the model.

2) *Configuration of Disparity Clip-Balanced Weight*: We explore the effectiveness of Disparity Clip-Balanced Weight. As shown in Table II, the utilization of Disparity Clip-Balanced Weight significantly improves the performance on multiple datasets. As mentioned previously, when the disparity error is split into multiple clips, the imbalance problem is shifted from the distribution of disparity between different domains to the distribution of disparity clips within the same domain. Therefore, our proposed stepwise regression architecture and Disparity Clip-Balanced Weight is an effective combination for achieving excellent performance.

3) *Number of Stepwise Regression Units*: In the practice of this paper, SR-Stereo remains essentially an iteration-based method. Therefore, our SR-Stereo can trade off efficiency and performance by adjusting the number of update units. As shown in Table III, SR-Stereo can achieve better performance for the same number of updates compared to the baseline, IGEV-Stereo. This result also shows that the range constraint on the update units does not reduce the convergence speed of the disparity, but rather makes the updated disparity more accurate.

4) *The Simplified Stepwise Regression Architecture*: Notably, the proposed stepwise regression architecture contains three key components: the Stepwise Regression Unit, Regression Objective Segment (ROS), and Disparity Clip-Balanced Weight (DCB). Except for the Stepwise Regression Unit, the

TABLE III

COMPARISON OF THE EFFICIENCY OF DISPARITY UPDATE UNITS ON DIFFERENT ARCHITECTURES. COMPARED WITH IGEV-STEREO, THE PROPOSED SR-STEREO ACHIEVES SIGNIFICANTLY BETTER DISPARITY ESTIMATION AND CROSS-DOMAIN GENERALIZATION WITH THE SAME NUMBER  $N$  OF UPDATES. **BOLD**: BETTER.

| Methods     | $N$ | SceneFlow   |             | Middlebury-H | ETH3D       |
|-------------|-----|-------------|-------------|--------------|-------------|
|             |     | EPE(px)     | > 3px       | > 2px        | > 1px       |
| IGEV-Stereo | 9   | 0.73        | 3.69        | 8.89         | 4.74        |
| SR-Stereo   |     | <b>0.72</b> | <b>3.32</b> | <b>7.66</b>  | <b>3.93</b> |
| IGEV-Stereo | 12  | 0.72        | 3.65        | 8.59         | 4.57        |
| SR-Stereo   |     | <b>0.71</b> | <b>3.26</b> | <b>7.31</b>  | <b>3.93</b> |
| IGEV-Stereo | 15  | 0.72        | 3.65        | 8.44         | 4.49        |
| SR-Stereo   |     | <b>0.70</b> | <b>3.23</b> | <b>7.17</b>  | <b>3.82</b> |
| IGEV-Stereo | 18  | 0.71        | 3.63        | 8.40         | 4.43        |
| SR-Stereo   |     | <b>0.70</b> | <b>3.22</b> | <b>7.22</b>  | <b>3.86</b> |
| IGEV-Stereo | 21  | 0.71        | 3.63        | 8.44         | 4.42        |
| SR-Stereo   |     | <b>0.70</b> | <b>3.22</b> | <b>7.15</b>  | <b>3.81</b> |
| IGEV-Stereo | 32  | 0.73        | 3.68        | 8.18         | 4.44        |
| SR-Stereo   |     | <b>0.71</b> | <b>3.24</b> | <b>7.14</b>  | <b>3.85</b> |

TABLE IV

EXTENSION RESULTS FOR THE SIMPLIFIED STEPWISE REGRESSION ARCHITECTURE. FOR INFERENCE, IGEV-STEREO RUNS 15 DISPARITY UPDATES, WHILE RAFT-STEREO RUNS 32 DISPARITY UPDATES. ROS:REGRESSION OBJECTIVE SEGMENT. DCB: DISPARITY CLIP-BALANCED WEIGHT ( $h=0.5$ ). GRAY: PERFORMANCE IS IMPROVED AFTER USING THE PROPOSED METHOD. **BOLD**: BEST.

| Methods       | $m$ | SceneFlow   | Middlebury-H | ETH3D       |
|---------------|-----|-------------|--------------|-------------|
|               |     | > 3px(%)    | > 2px(%)     | > 1px(%)    |
| IGEV-Stereo   | -   | 3.65        | 8.44         | 4.49        |
| IGEV.+ROS     | 2   | 3.50        | 8.09         | 4.40        |
|               | 3   | 3.48        | 8.06         | 4.71        |
|               | 4   | 3.48        | 8.10         | 4.37        |
| IGEV.+ROS+DCB | 2   | 3.32        | 7.68         | 3.87        |
|               | 3   | 3.26        | <b>7.61</b>  | 4.22        |
|               | 4   | <b>3.24</b> | 7.78         | <b>3.47</b> |
| RAFT-Stereo   | -   | 3.96        | 14.71        | 4.51        |
| RAFT.+ROS     | 3   | 4.25        | 15.78        | 3.86        |
|               | 4   | 4.01        | 14.42        | 4.02        |
|               | 5   | 3.76        | 12.26        | 4.13        |
| RAFT.+ROS+DCB | 3   | 3.70        | 13.97        | 3.60        |
|               | 4   | 3.56        | 12.64        | 3.63        |
|               | 5   | <b>3.42</b> | <b>11.88</b> | <b>3.59</b> |

other two do not involve changes in the network structure. To further demonstrate the plug-and-play of the architecture, we apply the proposed ROS and DCB to the iteration-based methods RAFT-Stereo and IGEV-Stereo.

TABLE V  
 QUANTITATIVE EVALUATION ON SCENEFLOW AND KITTI. OUR SR-IGEV RUN 16 DISPARITY UPDATES DURING INFERENCE. **BOLD**: BEST. UNDERLINE: SECOND. **BLUE**: THIRD. \*: THE BASELINE. **BOTTOM RIGHT CORNER**: PERCENTAGE IMPROVEMENT COMPARED TO THE BASELINE.

| Methods             | Years | SceneFlow                        | KITTI 2015  |                                  |             | KITTI 2012  |                                  |             |                                  | KITTI Time(s) |             |
|---------------------|-------|----------------------------------|-------------|----------------------------------|-------------|-------------|----------------------------------|-------------|----------------------------------|---------------|-------------|
|                     |       |                                  | D1-bg       | D1-fg                            | D1-all      | 2-noc       | 2-all                            | 3-noc       | 3-all                            |               | EPE-all     |
| PSMNet [5]          | 2018  | 1.09                             | 1.86        | 4.62                             | 2.32        | 2.44        | 3.01                             | 1.49        | 1.89                             | 0.6           | 0.41        |
| GANet [23]          | 2019  | 0.80                             | 1.48        | 3.46                             | 1.81        | 1.89        | 2.50                             | 1.19        | 1.60                             | 0.5           | 1.80        |
| GwcNet [6]          | 2019  | 0.98                             | 1.74        | 3.93                             | 2.11        | 2.16        | 2.71                             | 1.32        | 1.70                             | 0.5           | 0.32        |
| AcfNet [24]         | 2020  | 0.87                             | 1.51        | 3.80                             | 1.89        | 1.83        | 2.35                             | 1.17        | 1.54                             | 0.5           | 0.48        |
| RAFT-Stereo [9]     | 2021  | 0.56                             | 1.58        | 3.05                             | 1.82        | 1.92        | 2.42                             | 1.30        | 1.66                             | 0.5           | 0.38        |
| CREStereo [8]       | 2022  | -                                | 1.45        | 2.86                             | 1.69        | 1.72        | 2.18                             | 1.14        | 1.46                             | 0.5           | 0.41        |
| ACVNet [7]          | 2022  | 0.48                             | 1.37        | 3.07                             | 1.65        | 1.83        | 2.35                             | 1.13        | 1.47                             | 0.5           | 0.20        |
| DLNR [13]           | 2023  | 0.48                             | 1.37        | <b>2.59</b>                      | 1.76        | -           | -                                | -           | -                                | -             | 0.28        |
| Croco-Stereo [12]   | 2023  | -                                | 1.38        | 2.65                             | 1.59        | -           | -                                | -           | -                                | -             | 0.93        |
| UPFNet [14]         | 2023  | -                                | 1.38        | 2.85                             | 1.62        | 1.67        | <b>2.17</b>                      | 1.09        | 1.45                             | 0.5           | 0.25        |
| IGEV-Stereo* [10]   | 2023  | 0.47                             | 1.38        | 2.67                             | 1.59        | 1.71        | <b>2.17</b>                      | 1.12        | 1.44                             | <b>0.4</b>    | <b>0.18</b> |
| NMRF [34]           | 2024  | <b>0.45</b>                      | <b>1.28</b> | 3.13                             | 1.59        | <b>1.59</b> | <b>2.07</b>                      | <b>1.01</b> | <b>1.35</b>                      | -             | <b>0.09</b> |
| ADL-GwcNet [35]     | 2024  | 0.62                             | 1.42        | 3.01                             | 1.68        | <u>1.65</u> | <u>2.17</u>                      | <u>1.05</u> | 1.42                             | -             | -           |
| DKT-IGEV [36]       | 2024  | -                                | 1.46        | 3.05                             | 1.72        | -           | -                                | 1.22        | 1.56                             | -             | -           |
| MoCha-Stereo [33]   | 2024  | <b>0.41</b>                      | <b>1.36</b> | <b>2.43</b>                      | <b>1.53</b> | -           | -                                | <u>1.06</u> | <u>1.36</u>                      | <b>0.4</b>    | 0.34        |
| Selective-IGEV [11] | 2024  | <u>0.44</u>                      | <u>1.33</u> | 2.61                             | <u>1.55</u> | <b>1.59</b> | <b>2.05</b>                      | 1.07        | 1.38                             | <b>0.4</b>    | 0.24        |
| SR-IGEV(Ours)       | -     | <b>0.45</b> <small>-4.3%</small> | 1.37        | <u>2.49</u> <small>-6.7%</small> | <b>1.56</b> | <b>1.66</b> | <u>2.07</u> <small>-4.6%</small> | 1.09        | <u>1.36</u> <small>-5.6%</small> | <b>0.4</b>    | <b>0.19</b> |

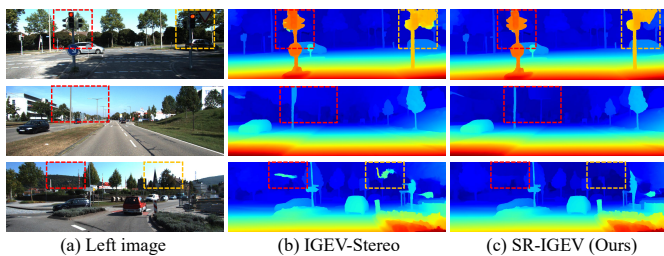


Fig. 10. Qualitative results on the test set of KITTI 2015. Both methods run 32 updates at inference. Our SR-IGEV is more accurate for edge regions and backgrounds.

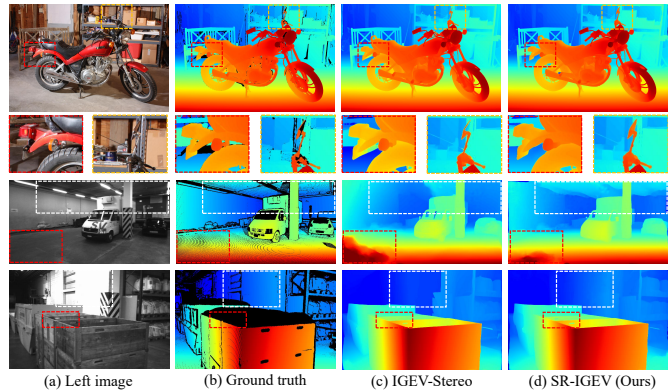


Fig. 11. Generalization results on Middlebury 2014 and ETH3D. All methods run 32 disparity updates during inference. Our SR-IGEV performs better in the background and detail regions.

As shown in Table IV, the ROS and DCB can improve the performance of existing iteration-based methods without changing the network structure, and therefore can be generalized very easily. In addition, we can adjust the disparity clip range  $m$  to achieve better results according to the characteristics of the existing methods. For instance, in the case of RAFT-Stereo, where the initial disparity is set to 0, a large clip range is required to accelerate the disparity convergence. Therefore, the best results are obtained with a clip range of  $m=5$ . Conversely, IGEV-Stereo obtains a coarse initial disparity through 3D-CNN, making a smaller clip range more suitable to achieve stable performance improvement.

#### D. Comparison with SOTA Methods

1) *Benchmark Results*: In this section, we compare SR-Stereo with the state-of-the-art methods published on SceneFlow and KITTI. As described in Section IV-B1, we train the SR-IGEV on SceneFlow for 200k steps. Then, we fine-tune the SR-IGEV on the KITTI for 50k steps. Table V shows the quantitative results. As shown in Table V, unlike the state-of-the-art generalized stereo method DKT-IGEV [36], our method does not deteriorate the in-domain performance of the baseline model. On the contrary, surprisingly, with a similar training strategy, our SR-IGEV achieves similar performance

to the state-of-the-art method Selective-IGEV [11]. More importantly, compared to the baseline IGEV-Stereo, our method only increases the time cost by 0.01s, which is far better than the two IGEV-based SOTA methods (Selective-IGEV [11] and MoCha-Stereo [33]). All these results effectively demonstrate the advantages of our method. Figure 10 shows a comparison of the qualitative results of SR-Stereo and IGEV-Stereo on KITTI 2015. Our method is more accurate for edge regions and backgrounds.

2) *Zero-shot Generalization*: We test the SR-IGEV directly on Middlebury, ETH3D and KITTI. As shown in Table VI, Our method achieves very competitive generalization performance. Compared with the baseline IGEV-Stereo, our method achieves an overall improvement. Moreover, compared to the majority of generalized stereo methods, our method achieves the best performance on Middlebury and ETH3D. The generalization performance of our method on KITTI is also very competitive among the methods of the last two years. We also point out that we recommend evaluating the generalization performance more objectively based on the results on Middlebury and ETH3D, as is done in IGEV-

TABLE VI

CROSS-DOMAIN GENERALIZATION EVALUATION. OUR SR-IGEV RUN 32 DISPARITY UPDATES DURING INFERENCE. WE PRE-TRAIN OUR MODEL ON SCENEFLOW AND TEST IT DIRECTLY ON MIDDLEBURY 2014, ETH3D AND KITTI. THE 2-PIXEL ERROR RATE IS USED FOR MIDDLEBURY 2014, 1-PIXEL ERROR RATE FOR ETH3D AND D1-ERROR FOR KITTI. **BOLD**: BEST. UNDERLINE: SECOND. \*: THE BASELINE. **BOTTOM RIGHT CORNER**: PERCENTAGE IMPROVEMENT COMPARED TO THE BASELINE.

| Methods             | Type        | Years | Middlebury                       |                                 | ETH3D                            | KITTI-12                 | KITTI-15               |
|---------------------|-------------|-------|----------------------------------|---------------------------------|----------------------------------|--------------------------|------------------------|
|                     |             |       | Half                             | Quarter                         |                                  |                          |                        |
| PSMNet [5]          | Normal      | 2018  | 15.8                             | 9.8                             | 10.2                             | 15.1                     | 16.3                   |
| GANet [23]          |             | 2019  | 13.5                             | 8.5                             | 6.5                              | 10.1                     | 11.7                   |
| DSMNet [15]         |             | 2020  | 13.8                             | 8.1                             | 6.2                              | 6.2                      | 6.5                    |
| STTR [4]            |             | 2021  | 15.5                             | 9.7                             | 17.2                             | -                        | -                      |
| RAFT-Stereo [9]     |             | 2021  | 8.7                              | 7.3                             | 3.2                              | 5.7                      | 5.5                    |
| IGEV-Stereo* [10]   |             | 2023  | 7.1                              | 6.2                             | 3.6                              | 5.2                      | 6.0                    |
| MoCha-Stereo [33]   |             | 2024  | <u>6.2</u>                       | <b>4.9</b>                      | 3.2                              | -                        | -                      |
| Selective-IGEV [11] |             | 2024  | 6.8                              | 6.6                             | 5.4                              | 5.6                      | 6.0                    |
| NMRF [34]           |             | 2024  | -                                | 7.5                             | 3.8                              | 4.2                      | 5.1                    |
| Graft-GANNet [37]   | Generalized | 2022  | -                                | -                               | 6.2                              | 4.9                      | <b>4.2</b>             |
| FC-DSMNet [38]      |             | 2022  | 12.0                             | 7.8                             | 6.0                              | 5.5                      | 6.2                    |
| HVT-GwcNet [39]     |             | 2023  | 10.3                             | -                               | 5.9                              | <u>3.9</u>               | 5.0                    |
| Mask-LacGwcNet [40] |             | 2023  | 16.9                             | -                               | 5.3                              | 5.7                      | 5.6                    |
| ADL-GwcNet [35]     |             | 2024  | 9.1                              | -                               | 3.8                              | 4.5                      | <b>4.2</b>             |
| DKT-IGEV [36]       |             | 2024  | 6.9                              | -                               | <u>3.1</u>                       | <b>3.8</b>               | <b>4.8</b>             |
| SR-IGEV(Ours)       | -           | -     | <b>6.0</b> <small>-15.5%</small> | <u>6.0</u> <small>-3.2%</small> | <b>3.0</b> <small>-16.7%</small> | 4.9 <small>-5.8%</small> | 5.7 <small>-5%</small> |

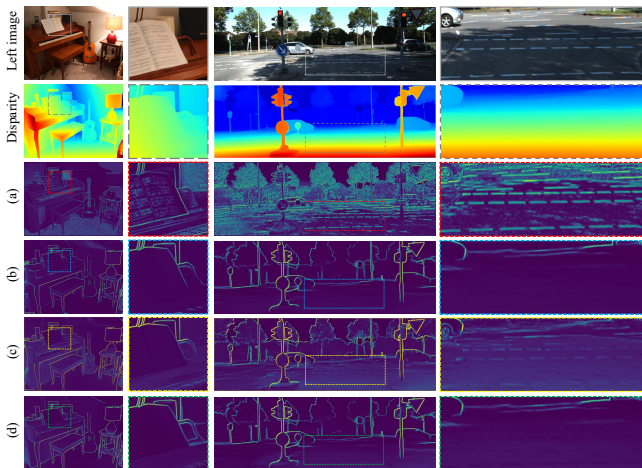


Fig. 12. Edge Estimation Results for Different Inputs. (a) Based on RGB image only. (b) Based on disparity only. (c) Based on concatenation of RGB image and disparity. (d) Step-by-step input of RGB image and disparity (Figure 8). All methods are trained on the SceneFlow using the same network architecture (i.e., two residual blocks in Figure 8). Test samples are obtained from Middlebury 2014 and KITTI-2015.

Stereo [10] and MoCha-Stereo [33]. Because the ground truth in KITTI is too sparse, which ignores errors in some regions. Finally, we visualize the generalization results of SR-IGEV in Figure 11. It can be seen that our method performs better in the background and detail regions.

E. Domain Adaptation based on Pre-trained Edge

As mentioned in Section III-A, in addition to proposing a robust network SR-Stereo, we also propose the DAPE to enhance the performance of existing models fine-tuned with sparse ground truth. In this section, we comprehensively evaluate the individual steps of DAPE and demonstrate its ef-

TABLE VII

DAPE FINE-TUNING RESULTS BASED ON DIFFERENT EDGE MAPS. THE BASELINE IS IGEV-STEREO AND IS FINE-TUNED ON THE SPARSIFIED GROUND TRUTH (SEE FIGURE 13 FOR MORE DETAILS). ED: EDGE DETECTION. †: BASED ON CONCATENATION OF RGB IMAGE AND DISPARITY. \*: STEP-BY-STEP INPUT OF RGB IMAGE AND DISPARITY (FIGURE 8). THE  $t = 0.25$  IN DAPE. **BOLD**: BEST.

| Methods  | ED Input |           | Middlebury   |             | ETH3D       |
|----------|----------|-----------|--------------|-------------|-------------|
|          | RGB      | Disparity | Full         | Half        |             |
| Baseline | -        | -         | 11.72        | 5.14        | 1.65        |
| DAPE     | √        | -         | 11.76        | 5.01        | 2.05        |
|          | -        | √         | 11.69        | <b>4.89</b> | 1.62        |
|          | √†       | √†        | <b>11.67</b> | 4.92        | 1.62        |
|          | √*       | √*        | 11.69        | 4.93        | <b>1.61</b> |

fectiveness through experimental results on KITTI, Middlebury and ETH3D.

1) *Different Inputs to the Edge Estimator*: We explore the impact of different inputs on performance while utilizing the same edge estimator structure (Figure 8). Figure 12 shows the qualitative results that highlight the differences between predicted edge maps obtained from different inputs. When only RGB images are used, the edge maps are excessively noisy due to the interference of object surface textures. In contrast, with the introduction of disparity, the noise in the edge map is significantly reduced. To further demonstrate the impact of edge detection on DAPE, we fine-tune IGEV-Stereo using different edge results. As shown in Table VII, the edge maps based only on RGB images worsen the effect of the DAPE architecture, which is particularly obvious on ETH3D. In addition, the three disparity-based edge maps do not show a significant difference in the DAPE architecture, and all of them improve the fine-tuning performance. However, considering the visualization in Figure 12 and the diversity of signal sources, we recommend using the approach in Figure 8.

2) *Threshold for Edge Pseudo-label Generation*: As mentioned in Section III-D2, erroneous disparity estimation in ill-posed regions can lead to incorrect edge maps. We propose

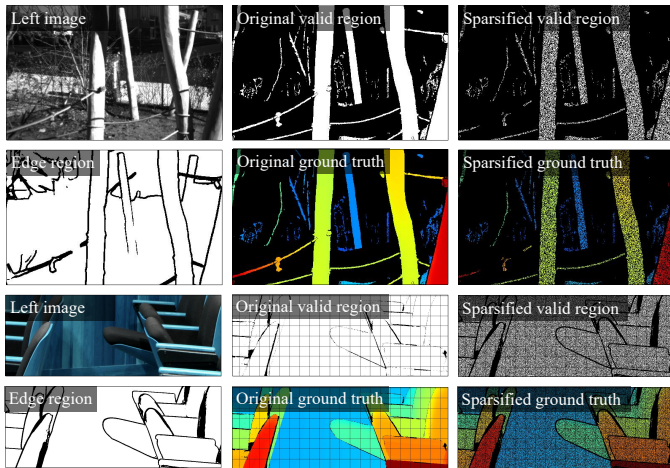


Fig. 13. Visualization of ground truth sparse process for ETH3D and Middbury 2014. First, we predict the edge map using the edge estimator proposed in Section IV-E1. Then, we remove the pixels in the edge region of the ground truth and randomly remove the pixels in the non-edge region with a probability of 0.5.

TABLE VIII

DOMAIN ADAPTATION EVALUATION OF DAPE ON ETH3D. WE EXPERIMENT WITH THE PROPOSED DAPE ON THREE MODELS. ALL METHODS ARE FINE-TUNED ON THE SPARSIFIED GROUND TRUTH AND EVALUATED ON THE ORIGINAL GROUND TRUTH. ALL METHODS RUN 15 DISPARITY UPDATES DURING INFERENCE. GRAY: PERFORMANCE IS IMPROVED AFTER USING DAPE. **BOLD**: BEST.

| Methods     | DAPE     | $> 1px$     | $> 0.75px$  | $> 0.25px$   | EPE(px)      |
|-------------|----------|-------------|-------------|--------------|--------------|
| RAFT-Stereo | -        | 3.46        | 4.47        | 20.74        | 0.315        |
|             | $t=0.25$ | 3.14        | 4.29        | 20.65        | 0.257        |
|             | $t=0.5$  | <b>2.94</b> | <b>4.18</b> | 20.79        | 0.256        |
|             | $t=0.75$ | 3.21        | 4.32        | 20.76        | <b>0.252</b> |
|             | $t=1.0$  | 2.98        | 4.26        | <b>20.59</b> | 0.255        |
| IGEV-Stereo | -        | 1.65        | 2.13        | 14.74        | 0.186        |
|             | $t=0.25$ | <b>1.61</b> | <b>2.12</b> | <b>14.65</b> | 0.182        |
|             | $t=0.5$  | 1.67        | 2.20        | 14.72        | <b>0.178</b> |
|             | $t=0.75$ | 1.68        | 2.18        | 14.90        | <b>0.178</b> |
|             | $t=1.0$  | 1.68        | 2.18        | 14.97        | 0.179        |
| SR-Stereo   | -        | 1.59        | 1.99        | 14.31        | 0.181        |
|             | $t=0.25$ | <b>1.52</b> | <b>1.97</b> | 14.23        | 0.177        |
|             | $t=0.5$  | 1.64        | 2.08        | 13.76        | 0.178        |
|             | $t=0.75$ | 1.66        | 2.09        | <b>13.74</b> | <b>0.174</b> |
|             | $t=1.0$  | 1.69        | 2.13        | 13.76        | 0.176        |

the use of threshold-based filtering to select pixels in non-edge region as pseudo-label. In this section, our focus is on exploring the threshold settings in different target domains. By doing so, we aim to analyze the impact of pseudo-label density on the adaptation of various domains. This analysis allows us to gain insights into the relationship between pseudo-label density and the effectiveness of DAPE.

*Results on ETH3D:* As mentioned in Section IV-A, we divide the ETH3D training pairs into two parts which are used for fine-tuning and evaluation respectively. To simulate the fine-tuning process on sparse ground truth, the ground truth of the part used for fine-tuning is randomly removed. Specifically, we remove the pixels in the edge region and randomly remove the pixels in the non-edge region with a probability of 0.5, as shown in Figure 13.

We utilize sparsified ground truth for model fine-tuning and the original ground truth for evaluation, ensuring a more

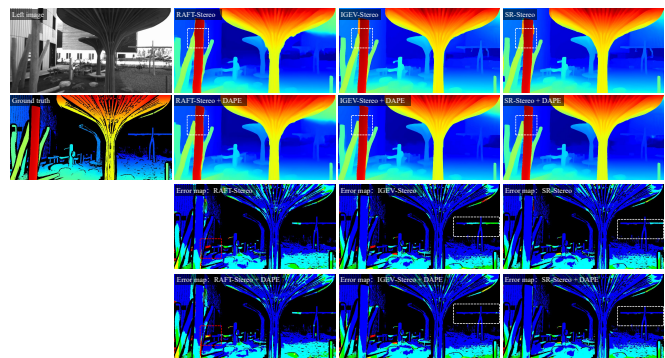


Fig. 14. Qualitative disparity estimation results of DAPE on ETH3D. All methods run 15 disparity updates during inference. The threshold  $t$  in DAPE is 0.25. In the error maps, red represents a larger error, while dark blue indicates a smaller error.

TABLE IX

DOMAIN ADAPTATION EVALUATION OF DAPE ON KITTI. WE EXPERIMENT WITH THE PROPOSED DAPE ON THREE MODELS. ALL METHODS RUN 15 DISPARITY UPDATES DURING INFERENCE. GRAY: PERFORMANCE IS IMPROVED AFTER USING DAPE. **BOLD**: BEST.

| Methods     | DAPE     | 3-noc       | 3-all       | EPE-noc      | EPE-all      |
|-------------|----------|-------------|-------------|--------------|--------------|
| RAFT-Stereo | -        | 1.17        | 1.37        | 0.483        | 0.507        |
|             | $t=0.25$ | 1.11        | 1.34        | 0.478        | 0.501        |
|             | $t=0.5$  | 1.14        | 1.38        | 0.479        | 0.506        |
|             | $t=0.75$ | <b>1.07</b> | 1.31        | <b>0.472</b> | <b>0.499</b> |
|             | $t=1.0$  | <b>1.07</b> | <b>1.29</b> | 0.474        | <b>0.499</b> |
| IGEV-Stereo | -        | 0.99        | 1.20        | 0.448        | 0.472        |
|             | $t=0.25$ | <b>0.96</b> | <b>1.16</b> | <b>0.445</b> | <b>0.468</b> |
|             | $t=0.5$  | <b>0.96</b> | 1.17        | <b>0.445</b> | 0.471        |
|             | $t=0.75$ | 0.97        | <b>1.16</b> | 0.446        | 0.471        |
|             | $t=1.0$  | 0.97        | 1.17        | 0.446        | 0.469        |
| SR-Stereo   | -        | 0.98        | 1.20        | 0.443        | 0.471        |
|             | $t=0.25$ | <b>0.95</b> | <b>1.16</b> | <b>0.440</b> | 0.468        |
|             | $t=0.5$  | 0.97        | 1.17        | 0.442        | <b>0.465</b> |
|             | $t=0.75$ | 0.97        | <b>1.16</b> | 0.443        | 0.469        |
|             | $t=1.0$  | 0.98        | <b>1.16</b> | 0.446        | 0.469        |

accurate assessment of the model’s domain-adaptive performance. The experimental results are presented in Table VIII. As the threshold  $t$  decreases in DAPE, the density of generated edge pseudo-labels decreases as well. When  $t$  is set to 0.25, all models exhibit performance improvement. This is due to the presence of reflective regions in some image pairs from ETH3D, which can lead to misleading edge map predictions. By using a smaller threshold, false edges are filtered out, resulting in more stable performance improvement. Figure 14 shows the qualitative results of DAPE for different models. It can be observed that our proposed DAPE effectively improves the performance of the model in the detail region.

*Results on KITTI:* Considering the limitation of the number of KITTI online leaderboard submissions, we have divided the KITTI training set into two parts, with a ratio of 4:1 for fine-tuning the model and evaluation, respectively. The dataset provides sparse ground truth disparities obtained from lidar measurements. Notably, the upper regions of KITTI images primarily consist of sky and distant objects, where ground truth disparities are not available. Moreover, lidar performs poorly in the edge regions of objects, resulting in a lack of ground truth disparities for pixels in these areas. These factors lead to

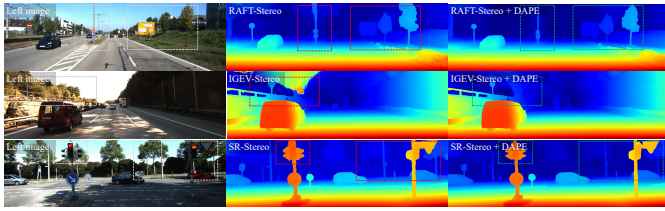


Fig. 15. Qualitative disparity estimation results of DAPE on KITTI test set. All methods run 15 disparity updates during inference. For RAFT-Stereo, the threshold  $t$  used for DAPE is 1, while for the other two models, it is 0.25.

TABLE X

DOMAIN ADAPTATION EVALUATION OF DAPE ON MIDDLEBURY 2014. ALL METHODS ARE FINE-TUNED ON THE SPARSIFIED GROUND TRUTH AND EVALUATED ON THE ORIGINAL GROUND TRUTH. DUE TO THE LARGE DISPARITY RANGE OF MIDDLEBURY 2014, RAFT-STEREO RUNS 32 DISPARITY UPDATES DURING INFERENCE, WHILE THE OTHER TWO MODELS RUN 15 DISPARITY UPDATES. WE USE THE 2-PIXEL ERROR AS THE EVALUATION METRIC. GRAY: PERFORMANCE IS IMPROVED AFTER USING DAPE. **BOLD**: BEST.

| Methods     | DAPE     | Full         | Half        | Quarter     |
|-------------|----------|--------------|-------------|-------------|
| RAFT-Stereo | -        | 12.85        | 8.14        | 7.56        |
|             | $t=0.25$ | 11.71        | 7.89        | 7.27        |
|             | $t=0.5$  | 11.56        | 7.89        | 7.02        |
|             | $t=0.75$ | 11.58        | <b>7.81</b> | 7.00        |
|             | $t=1.0$  | <b>11.47</b> | 7.84        | <b>6.87</b> |
| IGEV-Stereo | -        | 11.72        | 5.14        | 5.00        |
|             | $t=0.25$ | 11.69        | 4.93        | 4.99        |
|             | $t=0.5$  | <b>11.38</b> | 4.93        | 4.98        |
|             | $t=0.75$ | 11.49        | <b>4.82</b> | 4.86        |
|             | $t=1.0$  | 11.53        | 4.92        | <b>4.85</b> |
| SR-Stereo   | -        | 11.06        | 4.99        | 4.65        |
|             | $t=0.25$ | 10.97        | <b>4.81</b> | 4.62        |
|             | $t=0.5$  | <b>10.90</b> | 5.00        | 4.61        |
|             | $t=0.75$ | 11.02        | 4.97        | 4.58        |
|             | $t=1.0$  | 11.01        | 4.97        | <b>4.56</b> |

a mismatch between the accuracy ranking and the visualization on the KITTI online leaderboard. To ensure a more objective evaluation of the effectiveness of the proposed DAPE, we present the experimental results of DAPE on different models from both quantitative performance and visualization.

As shown in Table IX, the implementation of DAPE with most threshold values leads to performance improvements in both non-occluded and overall regions for all three models. Notably, the RAFT-Stereo model benefits significantly from higher-density edge pseudo-labels. Despite the presence of some erroneous labels in high-density edge pseudo-labels, they provide more comprehensive edge information, which effectively complements the edge disparity update guidance in RAFT-Stereo, especially considering its initial disparity is set to zero. Figure 15 showcases the qualitative results of DAPE on different models. Alongside enhancing the model’s performance in detailed regions, the proposed DAPE successfully mitigates disparity anomalies in textureless sky areas of the images.

*Results on Middlebury:* We use the additional 13 image pairs provided by Middlebury 2014 to fine-tune the models, and evaluate the domain adaptation performance using the original 15 training image pairs. Similar to the experiments conducted on ETH3D, we employ sparsified ground truth during the fine-tuning process, while relying on the original ground truth for

evaluation, as shown in Figure 13.

To verify the performance of DAPE at different resolutions, we evaluate it on Middlebury 2014 with three different resolutions. The qualitative results of DAPE on Middlebury 2014 are presented in Table X. Consistent with the conclusions from the previous two datasets, the implementation of DAPE with most threshold values leads to performance improvements of the three models. This outcome further confirms the generalizability and robustness of DAPE across different scenarios.

## V. CONCLUSION

In this paper, we propose a novel stereo method, SR-Stereo, and a novel fine-tuning framework, DAPE. SR-Stereo overcomes the domain discrepancies by predicting multiple range-controlled disparity clips to achieve better generalization performance and domain adaptation performance. Furthermore, for domain adaptation on sparse ground truth, the proposed DAPE uses generated edge pseudo-labels to provide additional supervision to the fine-tuned model. We have conducted extensive experiments on Sceneflow, KITTI, Middlebury, and ETH3D, and effectively demonstrated the advancements of SR-Stereo and the effectiveness of DAPE. Compared to the baseline, the proposed SR-Stereo achieves both better cross-domain performance and in-domain performance. This result is in complete contrast to many generalized stereo methods, which tend to have poor in-domain performance. In the future, we plan to implement a stereo method based entirely on stepwise regression by designing more components related to stepwise regression architecture.

## REFERENCES

- [1] Y. Zhang, Z. Xiong, Z. Yang, and F. Wu, “Real-time scalable depth sensing with hybrid structured light illumination,” *IEEE Transactions on Image Processing*, vol. 23, no. 1, pp. 97–109, 2013.
- [2] Y. Liu, X. Zhang, Y. Luo, Q. Hao, J. Su, and G. Cai, “Guard-net: Lightweight stereo matching network via global and uncertainty-aware refinement for autonomous driving,” *IEEE Transactions on Intelligent Transportation Systems*, vol. 25, no. 8, pp. 10 260–10 273, 2024.
- [3] Z. Feng, M. Li, M. Stolz, M. Kunert, and W. Wiesbeck, “Lane detection with a high-resolution automotive radar by introducing a new type of road marking,” *IEEE Transactions on Intelligent Transportation Systems*, vol. 20, no. 7, pp. 2430–2447, 2018.
- [4] Li, Z., Liu, X., Drenkow, N., Ding, A., Creighton, F.X., Taylor, R.H., Unberath, M.: Revisiting stereo depth estimation from a sequence-to-sequence perspective with transformers. In: Proceedings of the IEEE/CVF international conference on computer vision. pp. 6197–6206 (2021)
- [5] Chang, J.R., Chen, Y.S.: Pyramid stereo matching network. In: Proceedings of the IEEE conference on computer vision and pattern recognition. pp. 5410–5418 (2018)
- [6] Guo, X., Yang, K., Yang, W., Wang, X., Li, H.: Group-wise correlation stereo network. In: Proceedings of the IEEE/CVF conference on computer vision and pattern recognition. pp. 3273–3282 (2019)
- [7] Xu, G., Cheng, J., Guo, P., Yang, X.: Attention concatenation volume for accurate and efficient stereo matching. In: Proceedings of the IEEE/CVF Conference on Computer Vision and Pattern Recognition. pp. 12981–12990 (2022)
- [8] Li, J., Wang, P., Xiong, P., Cai, T., Yan, Z., Yang, L., Liu, J., Fan, H., Liu, S.: Practical stereo matching via cascaded recurrent network with adaptive correlation. In: Proceedings of the IEEE/CVF conference on computer vision and pattern recognition. pp. 16263–16272 (2022)
- [9] Lipson, L., Teed, Z., Deng, J.: Raft-stereo: Multilevel recurrent field transforms for stereo matching. In: 2021 International Conference on 3D Vision (3DV). pp. 218–227. IEEE (2021)
- [10] Xu, G., Wang, X., Ding, X., Yang, X.: Iterative geometry encoding volume for stereo matching. In: Proceedings of the IEEE/CVF Conference on Computer Vision and Pattern Recognition. pp. 21919–21928 (2023)

- [11] X. Wang, G. Xu, H. Jia, and X. Yang, "Selective-stereo: Adaptive frequency information selection for stereo matching," *arXiv preprint arXiv:2403.00486*, 2024.
- [12] Weinzaepfel, P., Lucas, T., Leroy, V., Cabon, Y., Arora, V., Brégier, R., Csurka, G., Antsfeld, L., Chidlovskii, B., Revaud, J.: Croco v2: Improved cross-view completion pre-training for stereo matching and optical flow. In: Proceedings of the IEEE/CVF International Conference on Computer Vision. pp. 17969–17980 (2023)
- [13] Zhao, H., Zhou, H., Zhang, Y., Chen, J., Yang, Y., Zhao, Y.: High-frequency stereo matching network. In: Proceedings of the IEEE/CVF Conference on Computer Vision and Pattern Recognition. pp. 1327–1336 (2023)
- [14] Shen, Z., Song, X., Dai, Y., Zhou, D., Rao, Z., Zhang, L.: Digging into uncertainty-based pseudo-label for robust stereo matching. *IEEE Transactions on Pattern Analysis and Machine Intelligence* (2023)
- [15] Zhang, F., Qi, X., Yang, R., Prisacariu, V., Wah, B., Torr, P.: Domain-invariant stereo matching networks. In: Computer Vision–ECCV 2020: 16th European Conference, Glasgow, UK, August 23–28, 2020, Proceedings, Part II 16. pp. 420–439. Springer (2020)
- [16] Mayer, N., Ilg, E., Hausser, P., Fischer, P., Cremers, D., Dosovitskiy, A., Brox, T.: A large dataset to train convolutional networks for disparity, optical flow, and scene flow estimation. In: Proceedings of the IEEE conference on computer vision and pattern recognition. pp. 4040–4048 (2016)
- [17] Scharstein, D., Hirschmüller, H., Kitajima, Y., Krathwohl, G., Nešić, N., Wang, X., Westling, P.: High-resolution stereo datasets with subpixel-accurate ground truth. In: Pattern Recognition: 36th German Conference, GCPR 2014, Münster, Germany, September 2-5, 2014, Proceedings 36. pp. 31–42. Springer (2014)
- [18] Menze, M., Geiger, A.: Object scene flow for autonomous vehicles. In: Proceedings of the IEEE conference on computer vision and pattern recognition. pp. 3061–3070 (2015)
- [19] Geiger, A., Lenz, P., Urtasun, R.: Are we ready for autonomous driving? the kitti vision benchmark suite. In: 2012 IEEE conference on computer vision and pattern recognition. pp. 3354–3361. IEEE (2012)
- [20] S. Dong, W. Zhou, C. Xu, and W. Yan, "Egfnets: Edge-aware guidance fusion network for rgb–thermal urban scene parsing," *IEEE Transactions on Intelligent Transportation Systems*, 2023.
- [21] T. Cao, Y. Wang, and S. Liu, "Pavement crack detection based on 3d edge representation and data communication with digital twins," *IEEE Transactions on Intelligent Transportation Systems*, vol. 24, no. 7, pp. 7697–7706, 2022.
- [22] J.-M. Guo, H. Markoni, and J.-D. Lee, "Barnet: Boundary aware refinement network for crack detection," *IEEE Transactions on Intelligent Transportation Systems*, vol. 23, no. 7, pp. 7343–7358, 2021.
- [23] Zhang, F., Prisacariu, V., Yang, R., Torr, P.H.: Ga-net: Guided aggregation net for end-to-end stereo matching. In: Proceedings of the IEEE/CVF Conference on Computer Vision and Pattern Recognition. pp. 185–194 (2019)
- [24] Zhang, Y., Chen, Y., Bai, X., Yu, S., Yu, K., Li, Z., Yang, K.: Adaptive unimodal cost volume filtering for deep stereo matching. In: Proceedings of the AAAI Conference on Artificial Intelligence. vol. 34, pp. 12926–12934 (2020)
- [25] K. Zeng, Y. Wang, Q. Zhu, J. Mao, and H. Zhang, "Deep progressive fusion stereo network," *IEEE Transactions on Intelligent Transportation Systems*, vol. 23, no. 12, pp. 25 437–25 447, 2021.
- [26] Teed, Z., Deng, J.: Raft: Recurrent all-pairs field transforms for optical flow. In: Computer Vision–ECCV 2020: 16th European Conference, Glasgow, UK, August 23–28, 2020, Proceedings, Part II 16. pp. 402–419. Springer (2020)
- [27] Cho, K., Van Merriënboer, B., Gulcehre, C., Bahdanau, D., Bougares, F., Schwenk, H., Bengio, Y.: Learning phrase representations using rnn encoder-decoder for statistical machine translation. *arXiv preprint arXiv:1406.1078* (2014)
- [28] Graves, A., Graves, A.: Long short-term memory. Supervised sequence labelling with recurrent neural networks pp. 37–45 (2012)
- [29] M. Sandler, A. Howard, M. Zhu, A. Zhmoginov, and L.-C. Chen, "Mobilenetv2: Inverted residuals and linear bottlenecks," in *Proceedings of the IEEE conference on computer vision and pattern recognition*, 2018, pp. 4510–4520.
- [30] A. Krizhevsky, I. Sutskever, and G. E. Hinton, "Imagenet classification with deep convolutional neural networks," *Communications of the ACM*, vol. 60, no. 6, pp. 84–90, 2017.
- [31] He, K., Zhang, X., Ren, S., Sun, J.: Deep residual learning for image recognition. In: Proceedings of the IEEE conference on computer vision and pattern recognition. pp. 770–778 (2016)
- [32] Schops, T., Schonberger, J.L., Galliani, S., Sattler, T., Schindler, K., Pollefeys, M., Geiger, A.: A multi-view stereo benchmark with high-resolution images and multi-camera videos. In: Proceedings of the IEEE conference on computer vision and pattern recognition. pp. 3260–3269 (2017)
- [33] Z. Chen, W. Long, H. Yao, Y. Zhang, B. Wang, Y. Qin, and J. Wu, "Mocha-stereo: Motif channel attention network for stereo matching," in *Proceedings of the IEEE/CVF Conference on Computer Vision and Pattern Recognition*, 2024, pp. 27 768–27 777.
- [34] T. Guan, C. Wang, and Y.-H. Liu, "Neural markov random field for stereo matching," in *Proceedings of the IEEE/CVF Conference on Computer Vision and Pattern Recognition*, 2024, pp. 5459–5469.
- [35] P. Xu, Z. Xiang, C. Qiao, J. Fu, and T. Pu, "Adaptive multi-modal cross-entropy loss for stereo matching," in *Proceedings of the IEEE/CVF Conference on Computer Vision and Pattern Recognition*, 2024, pp. 5135–5144.
- [36] J. Zhang, J. Li, L. Huang, X. Yu, L. Gu, J. Zheng, and X. Bai, "Robust synthetic-to-real transfer for stereo matching," in *Proceedings of the IEEE/CVF Conference on Computer Vision and Pattern Recognition*, 2024, pp. 20 247–20 257.
- [37] B. Liu, H. Yu, and G. Qi, "Graftnet: Towards domain generalized stereo matching with a broad-spectrum and task-oriented feature," in *Proceedings of the IEEE/CVF conference on computer vision and pattern recognition*, 2022, pp. 13 012–13 021.
- [38] J. Zhang, X. Wang, X. Bai, C. Wang, L. Huang, Y. Chen, L. Gu, J. Zhou, T. Harada, and E. R. Hancock, "Revisiting domain generalized stereo matching networks from a feature consistency perspective," in *Proceedings of the IEEE/CVF Conference on Computer Vision and Pattern Recognition*, 2022, pp. 13 001–13 011.
- [39] T. Chang, X. Yang, T. Zhang, and M. Wang, "Domain generalized stereo matching via hierarchical visual transformation," in *Proceedings of the IEEE/CVF Conference on Computer Vision and Pattern Recognition*, 2023, pp. 9559–9568.
- [40] Z. Rao, B. Xiong, M. He, Y. Dai, R. He, Z. Shen, and X. Li, "Masked representation learning for domain generalized stereo matching," in *Proceedings of the IEEE/CVF Conference on Computer Vision and Pattern Recognition*, 2023, pp. 5435–5444.
- [41] X. Song, X. Zhao, L. Fang, H. Hu, and Y. Yu, "Edgestereo: An effective multi-task learning network for stereo matching and edge detection," *International Journal of Computer Vision*, vol. 128, no. 4, pp. 910–930, 2020.

**Weiqing Xiao** received the B.S. degree from SHENYUAN Honors College of Beihang University in 2022. He is currently pursuing the master's degree in School of the School of Electronic and Information Engineering, Beihang University. His research interests include computer vision and 3D vision.

**Wei Zhao** received the B.S., M.S., and Ph.D. degrees from the School of Automatic Control, Northwestern Polytechnical University, Xi'an, China. She was a Post-Doctoral Researcher with Beihang University, where she is currently a Full Professor. Her main research interests are digital image processing, automatic target recognition, information fusion.